INTERNATIONAL ATOMIC ENERGY AGENCY
UNITED NATIONS EDUCATIONAL, SCIENTIFIC AND CULTURAL ORGANIZATION

INTERNATIONAL CENTRE FOR THEORETICAL PHYSICS
34100 TRIESTE (ITALY) - P.O.B. 586 - MIRAMARE - STRADA COSTIERA 11 - TELEPHONE: 2240-1
CABLE: CENTRATOM - TELEX 460892-1

SMR/388 - 35

SPRING COLLEGE IN MATERIALS SCIENCE
ON
'CERAMICS AND COMPOSITE MATERIALS'
(17 April - 26 May 1989)

POROUS MEDIA
(Lecture III - V)

F.BROUERS
Department of Physics
University of the West Indies
Kingston 7
Jamaica, W.I.

argent verre

$p = \frac{\text{volume des sphères argent}}{\text{volume total}}$

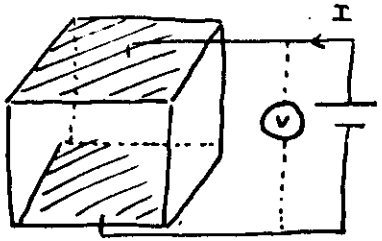

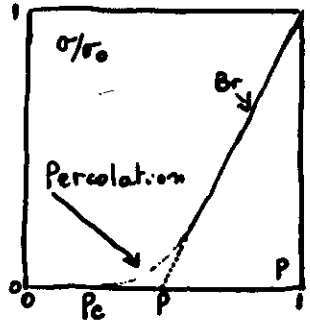

$p_c = 0.27$. (instead of 0.33)

on n'a plus la relation linéaire $\sigma/\sigma_0 \sim (p-p_c)^t$

t (3 dimensions) 1.7 → 1.98.

t (2 dimensions) $t \simeq 1.1$.

6 dimensions et $d > 6$ $t = 2$.

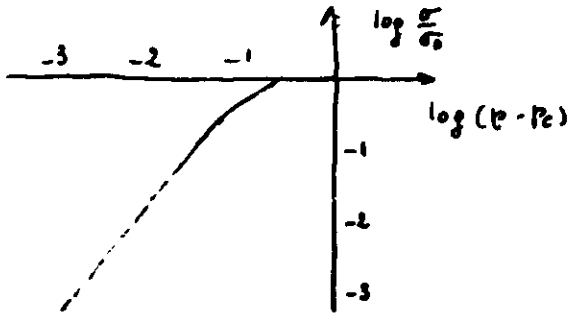

Percolation theory

p	σ
$1-p$	$\sigma = 0$

$$\sigma \sim (p-p_c)^t$$

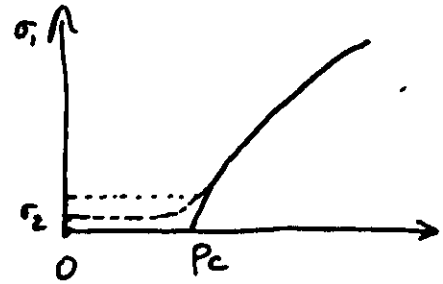

p	σ_1
$1-p$	$\sigma_2 \ll \sigma_1$

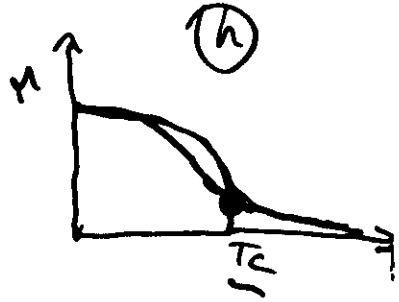

$$h \equiv \frac{\sigma_2}{\sigma_1}, \quad \frac{(T-T_c)}{T} \equiv \frac{p-p_c}{p}$$

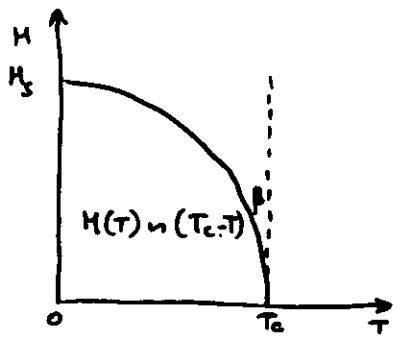

β 0.3 – 0.5

$\beta_{CM} = 1/2$

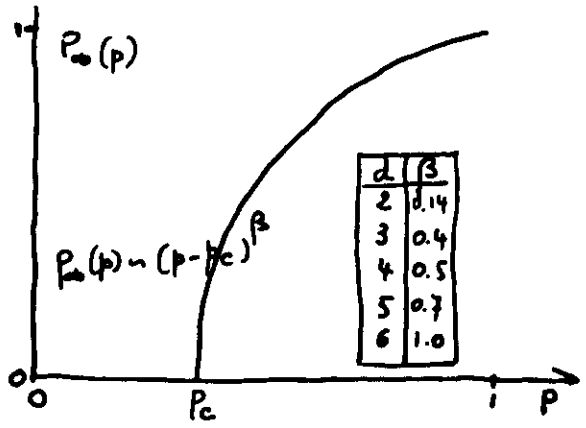

d	β
2	0.14
3	0.4
4	0.5
5	0.7
6	1.0

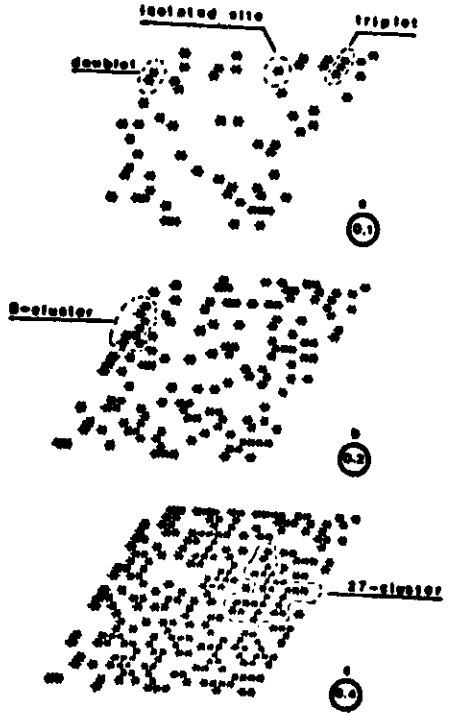

The size of the largest cluster increases with p.

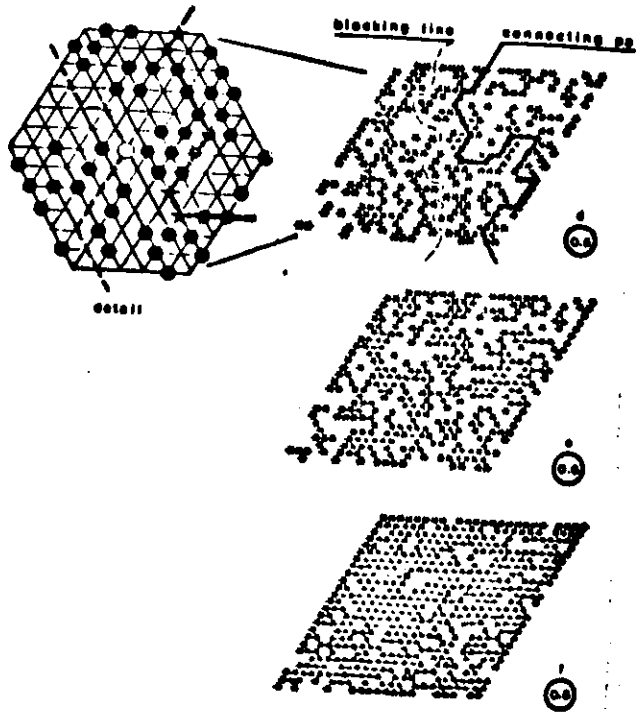

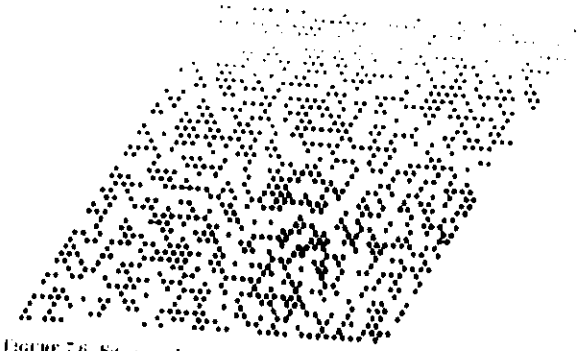

FIGURE 7.6 Site percolation clusters on the triangular lattice at the threshold $p_c = 1/2$.

FIGURE 7.7: (a) Clusters at p_c on a triangular lattice. (b) Coarse-graining of the triangular lattice by a factor $b = \sqrt{3}$. Occupied sites are shown as filled circles and open sites are shown as open circles. Groups of three sites are blocked as indicated by the shaded triangles. If a majority of the sites belonging to a triangle are occupied then the triangle is shaded dark. (c) The coarse-grained percolation lattice where filled sites correspond to dark triangles in (b).

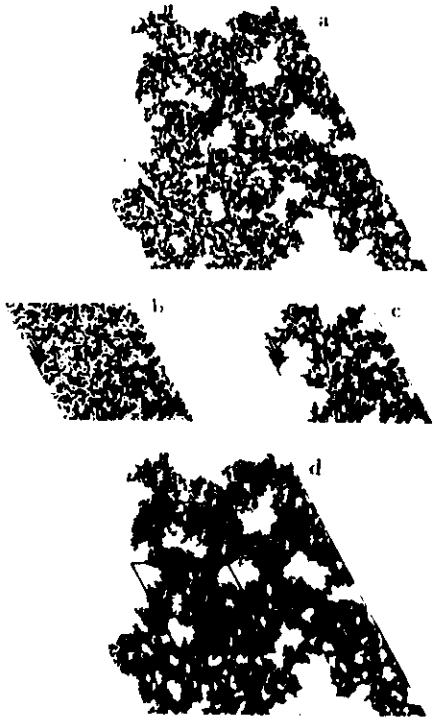

FIGURE 7.9. Self-similarity and the effect of coarse-graining on the triangular lattice at the percolation threshold. The scale is changed by a factor $b = 3$, using the renormalization procedure illustrated in figure 7.7 twice. (a) The percolation cluster at threshold on the original 180 × 180 lattice. (b) The occupied sites obtained after a scaling of the original lattice in (a) by a factor $b = 3$. (c) The percolation cluster of the scaled lattice in (b). (d) The scaled lattice is inserted into the original lattice in the region marked by a frame. The figure shows the resulting percolation cluster.

$p < p_c \qquad P_\infty = 0$

$p > p_c \qquad P_\infty \neq 0$

$p = p_c \qquad P_\infty \sim (p - p_c)^\beta$ ORDER PARAMETER

n_s average number/site of s-clusters $= \lim_{N\to\infty} \frac{N_s}{N}$

Average size $\qquad \frac{\sum s\, n_s}{\sum n_s}$

Mean average $\qquad \frac{\sum s^2 n_s}{\sum n_s} \sim |p - p_c|^{-\gamma}$

$$P_\infty + \sum_s n_s s = p$$

$\sum_s n_s \sim (p - p_c)^{2-\alpha}$ Free energy

$\sum_s s\, n_s \sim P_\infty(p) \sim (p - p_c)^\beta$ Magnetization

$\sum_s s^2 n_s \sim S(p) \sim (p - p_c)^{-\gamma}$ Susceptibility

$\xi \sim (p - p_c)^{-\nu}$ Correlation length

Mean distance between sites belonging to the same cluster.

Fortunately these exponent are related due to the existence of a SCALING LAW

$$n_s(p-p_c) = n_s(s, p-p_c)$$

not function of s and $(p-p_c)$ seperately

$$n_s(s, p-p_c) = s^{-\tau} f((p-p_c)s^{\sigma})$$

$$n_s(s, p_c) = s^{-\tau}$$

$$\frac{n_s(s, p-p_c)}{s^{-\tau}} = f(|p-p_c| s^{\sigma})$$

$$\frac{n_s(p)}{n_s(p_c)}, \frac{n_s(p)}{s^{-\tau}}$$

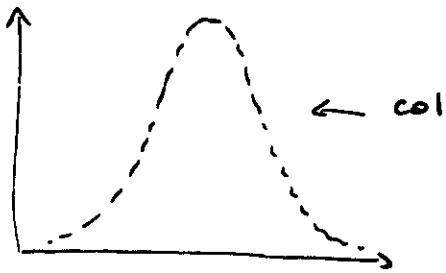

← collapse on one curve.

$|p-p_c| s^{\sigma}$

using this scaling law in the various expressions for the moment and integrating over s gave relation between various exponents

$$d\nu = \gamma + 2\beta \qquad \tau - \alpha = \frac{\tau - 1}{\sigma}$$

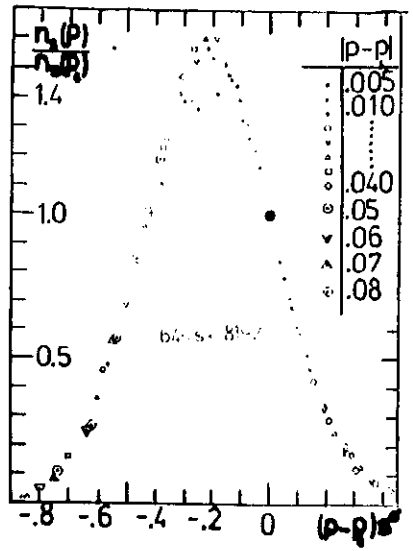

FIG. 9: Cluster numbers, normalized by their threshold values, versus the scaling variable s. Data for different p are seen to follow the same curve.

SELF. SIMILARITY AND FRACTALITY OF PERCOLATION CLUSTERS

1) below p_c

$$M(L) \sim L^D \qquad L \ll \xi$$
$$M(L) \sim \xi^D \qquad L \gg \xi$$

2) at p_c

$\xi \to \infty$ infinite self. similar cluster.

3) above p_c infinite cluster finite ξ
+ finite clusters in the empty space modelling the cluster

$\xi(p)$ is a typical distance up to which the infinite cluster is statistically self. similar

$M(L) \sim L^D \qquad L \ll \xi$

for $L \gg \xi \qquad M(L) \simeq \bar{\rho} L^d = P_\infty L^d \sim \xi^{D-d} L^d$

$$M(p, L) = L^D m(L/\xi) \qquad \xi \sim (p - p_c)^{-\nu}$$

$m(x \to 0) =$ constant

$m(x \to \infty) = \left(\frac{L}{\xi}\right)^{d-D}$

Since $P_\infty \sim (p - p_c)^\beta$

$\Rightarrow \beta = (d - D)\nu$

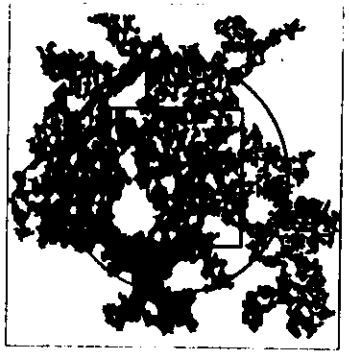

FIGURE 7.10. A finite cluster on the square lattice at p_c. The radius of the circle is the radius of gyration, $R_g(s) = 51$, of a cluster containing 6700 sites. The box indicated in the figure has a side $L = 60$. The side of the smallest box that contains the cluster is $L_s = 150$.

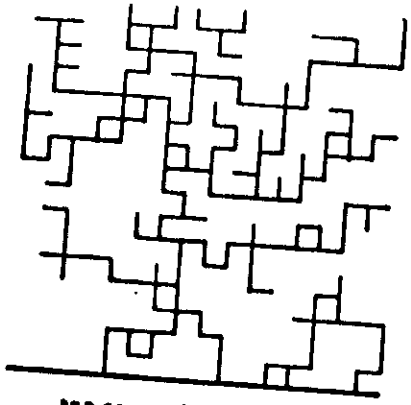

PERCOLATION CLUSTER

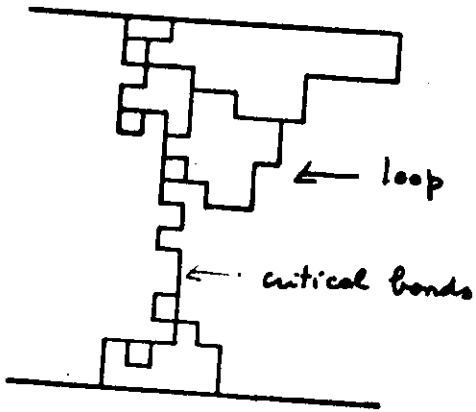

WITHOUT DEAD ARMS
(relevant for conductivity)

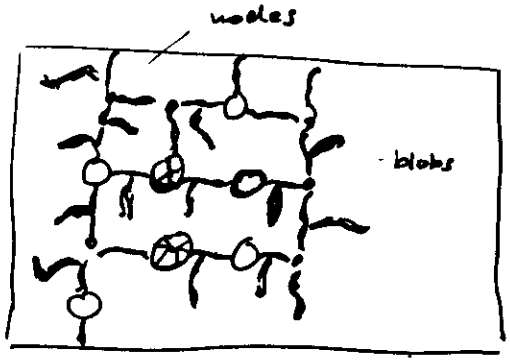

no dangling bonds backbone BB

$M_{BB}(L) \sim L^{D_{BB}}$

$N_{Red} \sim L^{D_{red}}$ $D_{red} = \frac{1}{\nu}$

$N_{blue} \sim L^{D_{blue}}$

$N_{yellow} \sim L^{D_{yellow}}$.

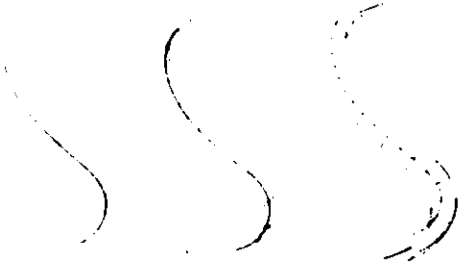

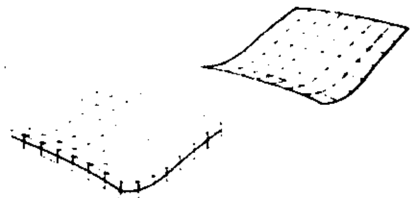

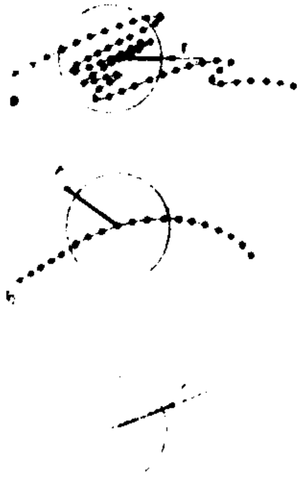

Figure VI.36.

Illustration de la méthode de calcul de la dimension fractale d'un ensemble de points.
Un cercle (ou sphère ou hypersphère) de rayon r est tracé en prenant pour centre un point quelconque de l'ensemble ; on détermine alors le nombre $N(r)$ de points situés à l'intérieur du cercle et sa variation en fonction de r.
a) cas général $N(r) \propto r$ [illegible]
b) ligne (dimension 1) $N(r) \propto r^1$
c) surface (dimension 2) $N(r) \propto r^2$
d) ensemble de Cantor $N(r) \propto r^{0.63}$...

$L(\delta) = a\,\delta^{1-D}$
$\delta \to 0$

From Jens. Feder — Fractals, Plenum 1988 ⇐ Recommended book

Length

$L = N(\delta)\,\delta \xrightarrow[\delta \to 0]{} L_0 \delta^0$

$A = N(\delta)\,\delta^2 \xrightarrow[\delta \to 0]{} L_0 \delta^1$

$V = N(\delta)\,\delta^3 \xrightarrow[\delta \to 0]{} L_0 \delta^2$

FIGURE 2.1: The coast of the southern part of Norway. The outline was traced from an atlas and digitised at about 1800 × 1200 pixels. The square grid indicated has a spacing of $\delta \sim 50$ km.

$$N(\delta) \sim \frac{1}{\delta^D}$$

$$M_\delta = \gamma(d)\, N(\delta)\, \delta^{d} \xrightarrow[\delta \to 0]{} \begin{cases} 0 & d > D \\ \infty & d < D \end{cases} \to \text{finite} \ldots$$

there is a jump in $d = D$

$$\delta^{1-\frac{\ln 4}{\ln 3}} = \delta^{\frac{\ln 3 - \ln 4}{\ln 3}}$$

$$= \exp \ln \delta^{\frac{\ln 3 - \ln 4}{\ln 3}}$$

$$= \exp \left(\frac{\ln 3 - \ln 4}{\ln 3} \right) \ln \delta$$

$$= \exp - \frac{\ln \delta \, [\ln 4 - \ln 3]}{\ln 3}$$

$$\left(\frac{4}{3}\right)^{\eta} = \left(\frac{4}{3}\right)^{-\frac{\ln \delta}{\ln 3}} = \exp \ln \left(\frac{4}{3}\right)^{-\frac{\ln \delta}{\ln 3}}$$

$$= \exp \left[- \frac{\ln \delta}{\ln 3} \ln \frac{4}{3} \right]$$

$$= \exp \left[- \frac{\ln \delta \, [\ln 4 - \ln 3]}{\ln 3} \right]$$

$$= \frac{\ln 4}{\ln \frac{1}{3}} = - \frac{\ln N}{\ln (r(N)}$$

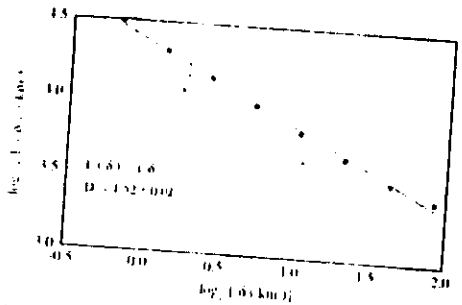

FIGURE 2.2. The measured length of the coastline shown in figure 2.1, as a function of the size δ of the $\delta \times \delta$ squares used to cover the coastline on the map. The straight line in this log-log plot corresponds to the relation $l(\delta) = a \cdot \delta^{1-D}$, with $D \simeq 1.52$.

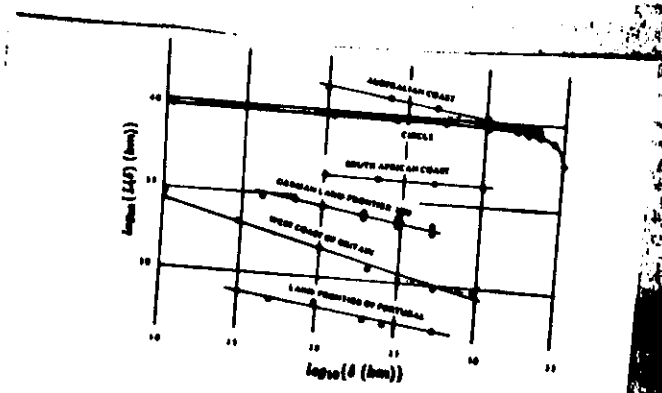

DETERMINISTIC FRACTAL

$L(1/3) = 4/3 \qquad L(1/9) = (4/3)^2 \qquad L(1/27) = (4/3)^3$

$L(\delta_n) = (4/3)^n \qquad \delta_n = 3^{-n} \qquad n = -\frac{\ln \delta_n}{\ln 3}$

Reduce /3
Cover with 4

$L(\delta_n) = (4/3)^{-\frac{\ln \delta_n}{\ln 3}}$

$= \delta^{1-D}$

Reduce $/3^n$
Cover with 4^n

$L(\delta) = N(\delta)\,\delta$

$N(\delta) = \delta^{-D}$

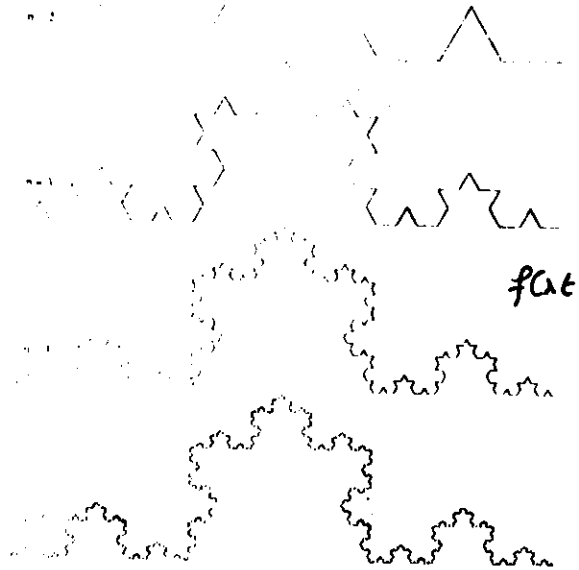

Scaling

$f(\lambda t) = \lambda^{\alpha} f(t)$

$\alpha = 1; \quad \lambda = (\frac{1}{3})$

$D = -\frac{\ln 4}{\ln \frac{1}{3}} = -\frac{\ln N}{\ln(r(N))}$

Scaling factor.

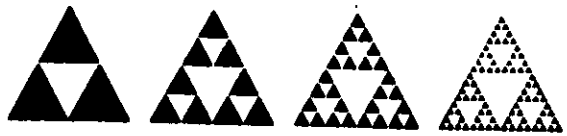

FIGURE 2.15: Construction of the triangular Sierpinski gasket. The initiator is a filled triangle. The generator eliminates a central triangle as shown. The fourth generation of the prefractal is shown to the right. The fractal curve obtained in the limit of an infinite number of generations has the fractal dimension $D = \ln 3/\ln 2 = 1.86\ldots$.

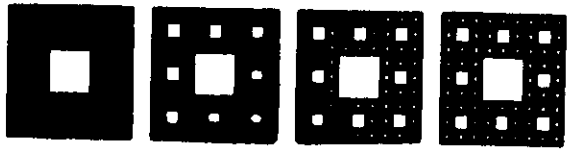

FIGURE 2.16: Construction of the Sierpinski carpet. The initiator is a square and the generator (shown on the left-hand side) is made of $N = 8$ squares. They are obtained by contractions of ratio $r = 1/3$. The right-hand side of the figure shows the fourth construction stage. The similarity dimension is $D = \ln 8/\ln 3 = 1.89\ldots$.

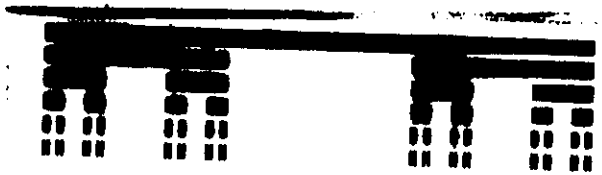

FIGURE 8.1: Construction of the triadic Cantor set. The initiator is the unit interval $[0, 1]$. The generator removes the open middle third. The figure shows the construction of the five first generations. $D = \ln 2/\ln 3 = 0.6309$.

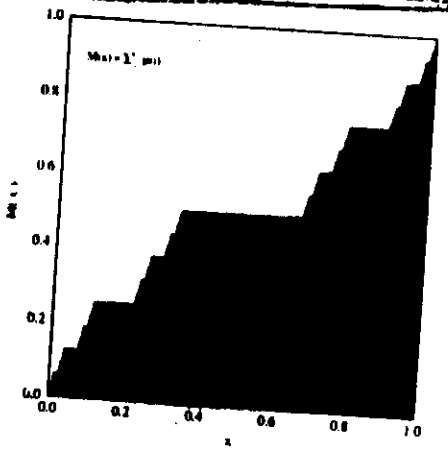

FIGURE 8.2: The mass of the triadic Cantor bar as a function of position along the bar. The curve is called a *Devil's staircase*.

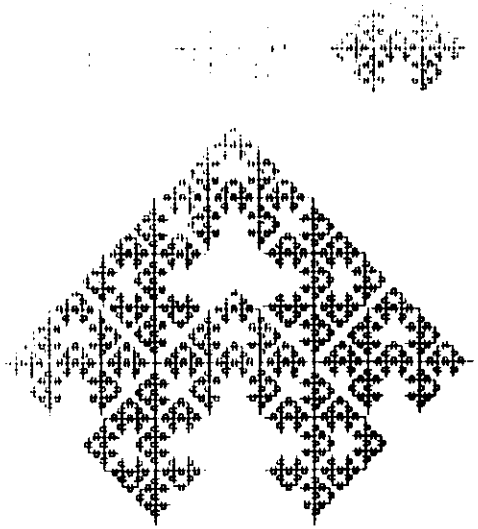

FIGURE 2.13: An implementation of the Mandelbrot-Given curve. Note that the height of the generator has been reduced slightly so that the structure of the curve becomes apparent. The fractal dimension is $D_B = \ln 8/\ln 3 = 1.89\ldots$ Mandelbrot and Given (1984) also describe random variants of this curve.

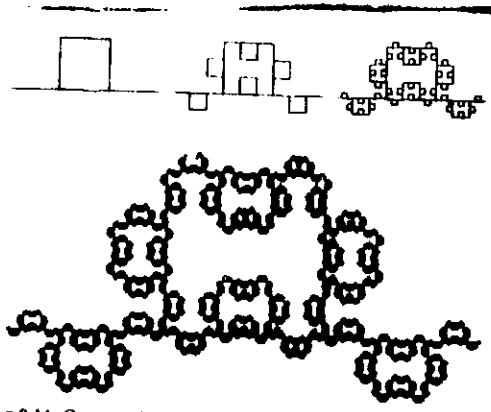

FIGURE 2.14: Construction of a Mandelbrot-Given curve without branches. This curve is obtained using a generator with a single loop. The fractal dimension is $D_B = \ln 6/\ln 3 = 1.63$.

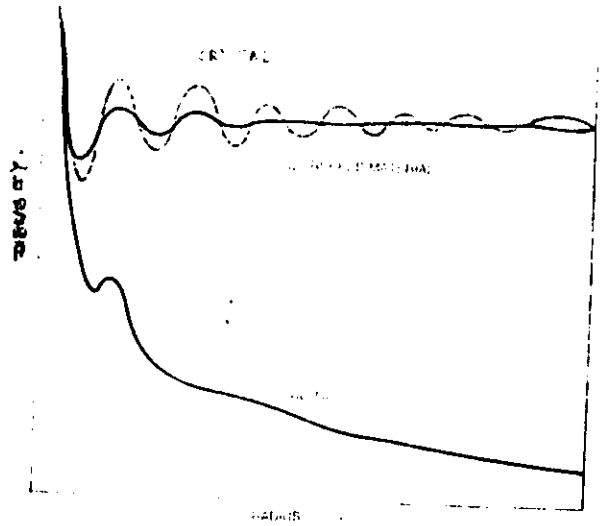

DENSITY OF A FRACTAL decreases with increasing size, as shown here. The densities of both ordered crystals and amorphous blobs, in contrast, approach fixed constants.

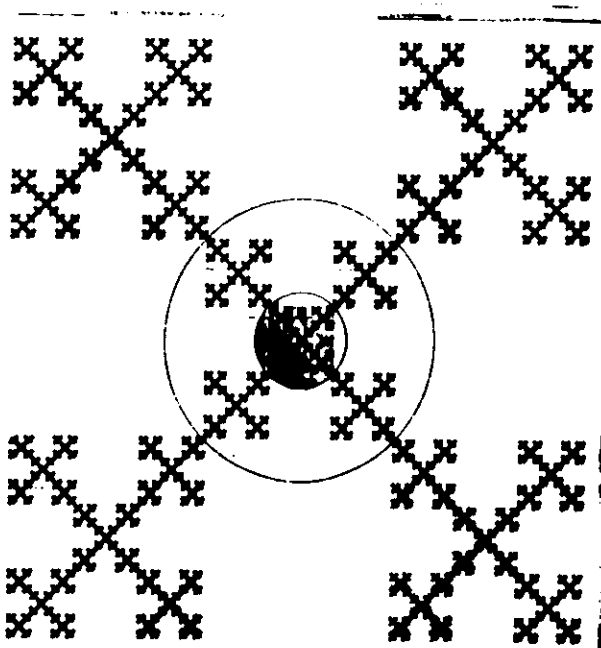

FRACTAL DIMENSION differs from an ordinary dimension in that it is not expressed as a whole number but as a fraction. To determine the precise fractal dimension of an object one counts the average number N of fundamental units of repetition found within a sphere of a certain radius r centered somewhere on the object. According to Euclidean geometry, the number of fundamental units then equals a constant C multiplied by the radius raised to the value of the dimension D ($N = C \cdot r^D$). In the case of a line the dimension is, of course, 1: tripling the radius of the sphere triples the number of units inside (*top left*). For ordinary (nonfractal) bulk matter in two dimensions, tripling the radius of the sphere multiplies the number of units by 9 (*top right*). For a fractal of dimension 1.46 (*bottom*), in contrast, tripling the radius multiplies the number of units by 5. In other

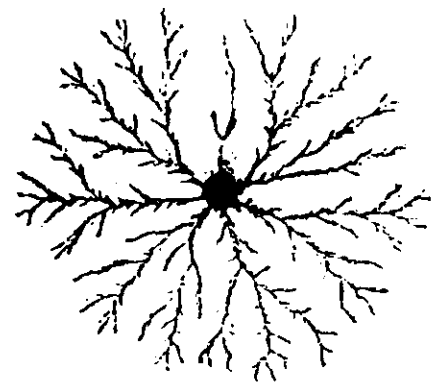

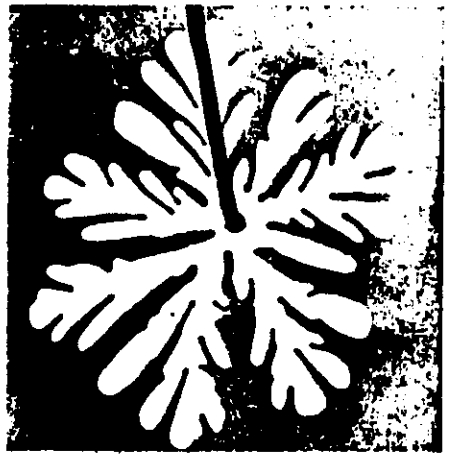

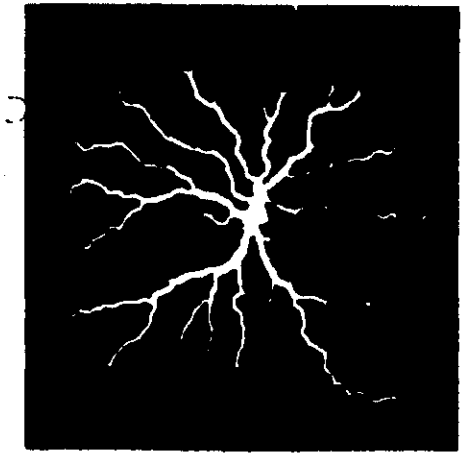

FRACTALS IN NATURE appear to grow by means of diffusion-limited aggregation. Shown here are a zinc deposit formed in an electrolytic cell (*top left*), a "viscous fingering" pattern of an air bubble in glycerine (*top right*) and an electrical-discharge pattern called a Lichtenberg figure (*bottom left*). The thick line that ends at the center of the bubble is an air tube. The zinc cluster at the bottom right shows what happens when the voltage in the electrolytic cell is increased: the growth pattern shifts from a fractal pattern to a dendritic, or snowflakelike, pattern. The zinc deposits were produced by Grier and the viscous-fingering pattern was produced by Eshel Ben-Jacob of the University of Michigan. The Lichtenberg figure is from L. Niemeyer and H. J. Wiesmann of Brown, Boveri & Company, Limited, in Switzerland, and Luciano Pietronero of the State University at Groningen.

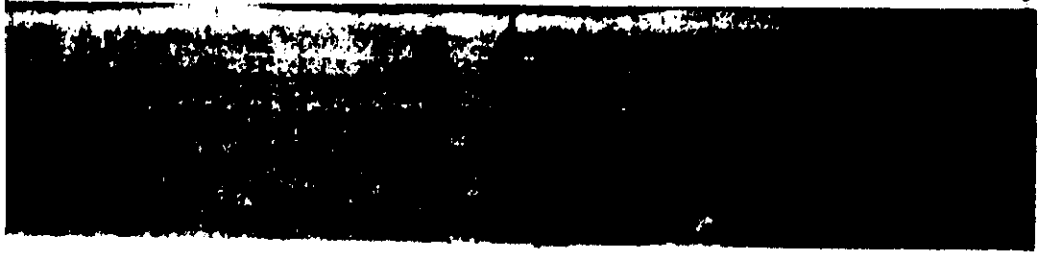

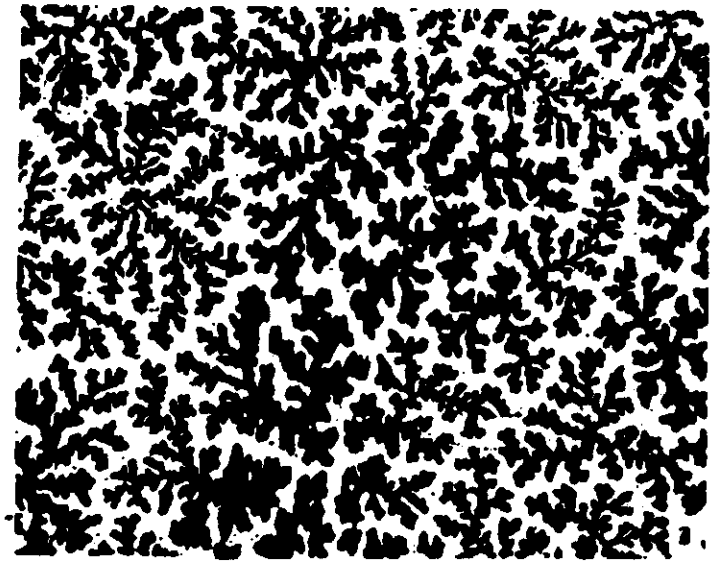

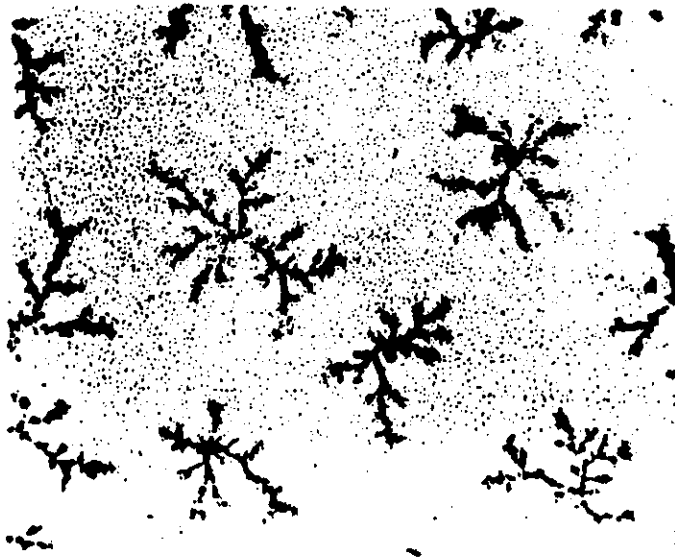

Fig. 3.5. A system-spanned $NbGe_2$ film on a SiO_2 surface. The film shown in (a) and (b) were formed under slightly different conditions (Ekin *et al.*, 1980). The figure was provided by S. A. Wolf and is reproduced with permission.)

ucture formed by the dissolution of plaster of Paris
a hole drilled into a block. The dissolution pattern
d and the remaining plaster of Paris was then dissolv
ed by G. Daccord and is reproduced with the permi
ger.

FIG. 3.9. A three-dimensional pattern formed by injecting water
cylinder of plaster of Paris (with zero flux boundary conditions
cylinder). This figure shows a Wood's metal replica of the
was provided by G. Daccord. [The figure is reproduced with
Dowell Schlumberger.]

(a) ... n early stage in the growth of a thick ...

DLA and the Harmonic Measure

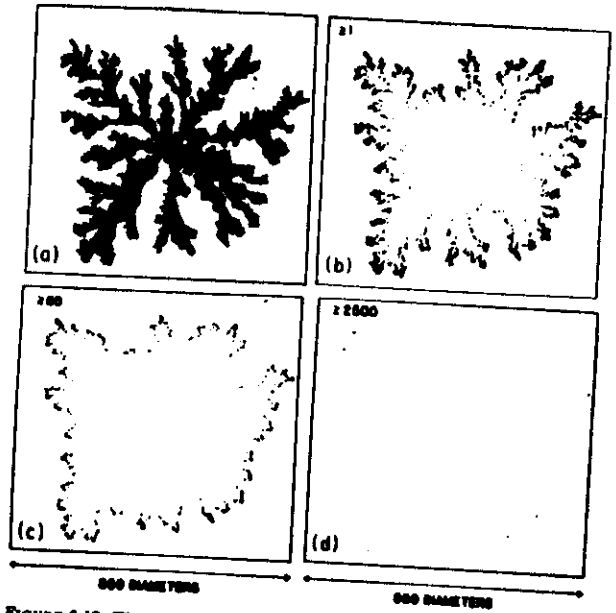

FIGURE 6.12: The result of a simulation in which 10^6 random walk particles were used to probe the surface of a two-dimensional off-lattice DLA cluster. After a particle had contacted the cluster, it was removed and a new particle started on a random walk trajectory from a random position on a circle enclosing the cluster. (a) The DLA cluster containing 50,000 particles. (b–d) show the location of the particles in the cluster which were contacted at least once, ≥ 50 times and ≥ 2500 times (Meakin et al., 1986).

How can we best characterize the surface of a perimeter of such fractal structure ?

Harmonic measure gives a method of qualitatively characterizing such surfaces

This (probability) measure is defined (with respect to a particular cluster) as the probability $p(r)dr$ of a random walker approaching the cluster from infinity first striking the cluster between r et $r+dr$ along the boundary of the cluster.

In practice one start from a DLA simulation one stops it.
It has no loops and the number of sites in the perimeter N_p (= number of possible growth sites)
$\sim N \sim L^D$ $\quad D = 1.71$.

The possible growth sites on the perimeter of the DLA are numbered with the index $k = 1, \dots N_p$
Further Simulation $\Rightarrow$ Probability of a random walker contacting the k-th site of the perimeter is $p_k = \frac{w_k}{\sum w_k}$

The set of probabilities

$$\mathcal{H} = \{p_k\}_{k=1}^{N_p} \quad \text{harmonic measure}$$

H_δ at the resolution of δ corresponding to the diameter of the diffusion particles.

One defines the quantity

$$N(q, L) = \sum_k p_k^q \sim \left(\frac{\delta}{L}\right)^{-\tau(q)} \sim L^{\tau(q)}$$

$q = 1 \qquad \sum_k p_k = 1 \qquad \tau(q)$ mass exponent.

for $q \gg 0$ the tips have the highest probability
for $q \ll 0$ the bottom of the fjords
for $q = 0 \qquad p_k^0 = 1 \qquad \sum_k p_k^0 = N(q=0, L) = L^{\tau(0)}$

$$= L^{D=1.71}$$

$\sum p_k^1 = 1 \Rightarrow \tau(1) = 0$

$\tau(q)$ varies from $-\infty$ to $+\infty$ when q varies from $+\infty$ to $-\infty$.

One defines $\alpha = -\frac{d\tau(q)}{dq}$

$$f = q\alpha + \tau(q)$$

The maximum of $f(\alpha)$ is D

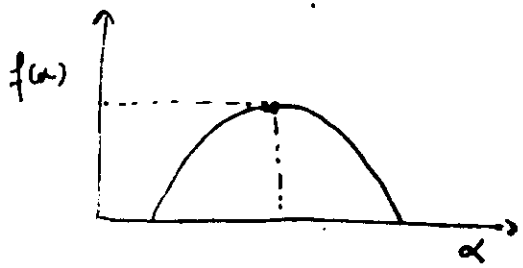

This curve characterizes the <u>measure</u> and is equivalent to the sequence of mass exponents $\tau(q)$

Laplace Equation

<u>D.L.A. process</u> : problem in which particles are left to wander at random until they reach the "surface" of the cluster where they come to rest and thus make the surface grow one step at the point of attachement

The random walkers are described by a diffusion equation

$$\frac{\partial C(r,t)}{\partial t} = \mathcal{D}\,\nabla^2 C(r,t)$$

with a steady sufly $\nabla^2 C(r,t) = 0$

A locally smooth boundary moves with a velocity

$$V_\perp = -\mathcal{D}\,\vec{n}\cdot\nabla c\,|_s$$

Randomness give rise to fractal growth.

<u>Viscous fingering</u> why similarity with DLA ?

Problem of viscous fingering in porous media is of central importance in oil recovery.

Fingering is due to an instability of the diffusive front when a high-viscosity fluid (oil) is displaced by a low-viscosity fluid (water or gas)

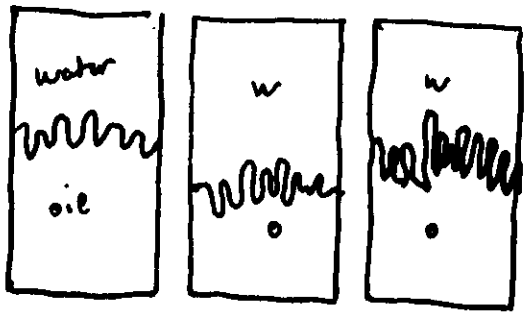

It is fractal in porous rocks. why Similar to DLA.
both problems are described by the Laplace equation.

The flow of a fluid in a porous medium is described by Darcy's equation.

$U = -\kappa \nabla \phi$ → flow potential (∇p)

↓ flow velocity

$\kappa = \frac{k}{\mu}$ → permiability of mat.

→ viscosity of fluid

For <u>incompressible</u> fluid $\nabla U = 0 \Rightarrow \nabla^2 \phi = 0$

(Laplace equation)

The displacement front moves with velocity

$\kappa \nabla \phi$

WHAT CREATES THE FRACTAL STRUCTURE IS THAT $\nabla \phi$ IS NOT DUE TO THE ABSOLUTE VALUE OF THE PRESSURE DIFFERENCE BUT THE CAPILLARITY PRESSURE ASSOCIATED WITH THE PORE NECK LEADING TO THE PORE

SINCE THE PORE NECK ARE <u>RANDOM</u> WITH SOME SIZE DISTRIBUTION.

CONCLUSION

THE DYNAMIC OF VISCOUS FINGERING FRONT IN POROUS MEDIA THEREFORE HAS TWO MAIN COMPONENTS

THE GLOBAL PRESSURE DISTRIBUTION CONTROLLED BY DARCY'S LAW AND THEREFORE THE LAPLACE EQUATION

AND THE LOCAL FLUCTUATIONS IN PORE GEOMETRY.

THE RESULT OF THOSE TWO FACTORS IS A GROWING FRACTAL STRUCTURE.

DIELECTRIC BREAKDOWN

$\nabla^2 \phi = 0$ ϕ IS THE ELECTRICAL POTENTIAL

$\phi = 0$ IN THE CONDUCTING PHASE

GROWTH VELOCITY $\propto \vec{E} = -\nabla \phi$.

METHODS TO MEASURE THE FRACTAL D OF A SURFACE

① Number of molecules of radius r per adsorbed monolayer on the surface. is

$$N(r) \propto r^{-D}$$

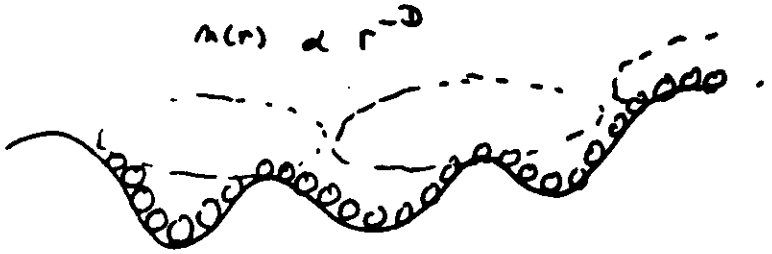

② Surface area as measured by r (from Nitrogen desorption isotherm)

$$A(r) \propto r^{2-D}$$

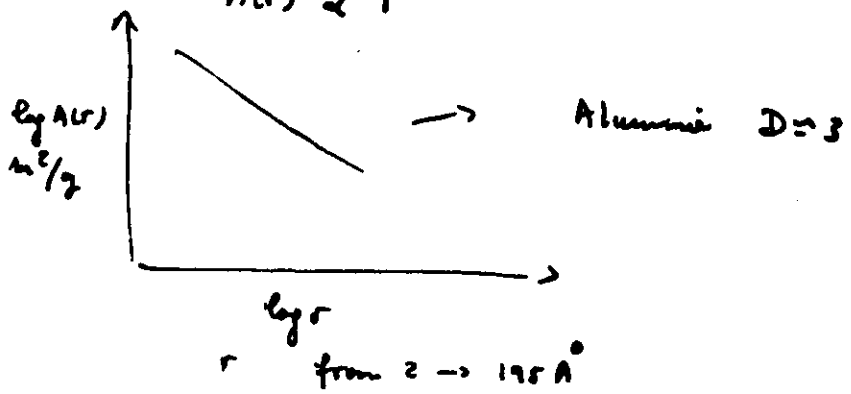

③ Velocity of reactions between Solids and Liquids is proportional to the area of contact

NON FRACTAL SURFACES WERE FOUND TO BE THE EXCEPTION RATHER THAN THE RULE

AVNIR et al. J. of Colloid and Interface Science

Fractal dimension*	Found in	At the range (Å)†
High		
2.91 ± 0.02	Upper Columbus dolomatic rock from Bellevue, Ohio	20–47,000
2.97 ± 0.01	Goodland high calcium rock, from Idabel, Okla.	20–47,000
2.88 ± 0.02	Granitic rock from SHOAL nuclear test site, Nevada	16–16,500
2.73 ± 0.05	Igneous rock sample from SHOAL site	16–14,300
2.71 ± 0.14	Granular activated carbon–Tsurumi HC-8, from coconut shell	(16–37)
2.80 ± 0.16	Granular activated carbon—Fujusawa B-CG, from coconut shell	(16–37)
2.90 ± 0.01	Carbonate rock from groundwater test well, Yucca Flat, Nevada	16–16,500
2.92 ± 0.02	Soil (kaolinite, trace halloysite)	150–16,500
2.94 ± 0.04	Porous silicic acid	(16–34)
2.79 ± 0.03	Activated alumina grade F-20 (Alcoa Corp.)	16–45,100
2.78 ± 0.21	Charcoal (BDH) of animal origin	1,400–180,000
2.67 ± 0.16	Porous coconut charcoal (Standard Chemical Co., Montreal)	(16–47)
Medium		
2.57 ± 0.04	Porous α-FeOOH pigment for magnetic tapes	16–980
2.35 ± 0.11	Crushed Corning 0010 lead glass	21–14,900
2.52 ± 0.07	Coal mine dust from Western Pennsylvania	16–180
2.33 ± 0.08	Coal mine dust from Western Pennsylvania	16–270
2.25 ± 0.09	Carbon black	(16–71)
2.54 ± 0.12	Slightly porous coconut charcoal (Standard Chemical Co., Montreal)	(16–47)
2.30 ± 0.07	Slightly porous coconut charcoal (Standard Chemical Co., Montreal)	(16–47)
2.63 ± 0.03	Mosheim high calcium from Stephens City, Va.	20–47,000
2.58 ± 0.01	Niagara (Guelph) dolomite from Woodville, Ohio	20–47,000
2.46 ± 0.11	Glassy melted rock from Rainier nuclear zone, Nevada	14–14,300
2.29 ± 0.06	Soil (mainly feldspar quartz and limonite)	150–21,800
Low		
2.02 ± 0.06	Aerosil—nonporous fumed silica (Degussa)	16–529
2.15 ± 0.06	Suprasil—ground fine Belgian quartz glass of high purity	16–10,600
2.14 ± 0.06	Madagascar quartz from Thermal Syndicate	16–1,850
1.95 ± 0.04	Periclase—electrically fused and crushed magnesite	16–720
2.02 ± 0.05	Synthetic faujasite ($Na_2O \cdot Al_2O_3 \cdot 2.67SiO_2 \cdot mH_2O$) (Linde Air Products)	(16–68)
2.07 ± 0.01	Graphite—Vulcan 3G (2700) (National Physical Lab., Teddington, UK)	(16–178)
2.04 ± 0.16	Graphon—partially graphitized carbon black formed by heating MPC black to 3,200 °C	(15–41)
2.13 ± 0.16	Graphon—graphitized carbon black (Cabot Corp.)	1,400–180,000
2.04 ± 0.04	Active, (nonporous), coconut charcoal (Standard Chemical Co., Montreal)	(16–47)
1.97 ± 0.02	Active, (nonporous), coconut charcoal (Standard Chemical Co., Montreal)	(16–47)
2.16 ± 0.04	Iceland spar, massive calcite from Chihuahua, Mexico	20–47,000

FIGURE 14.8: Fractal dimensions of surfaces measured by molecular adsorption (Avnir et al., 1984).

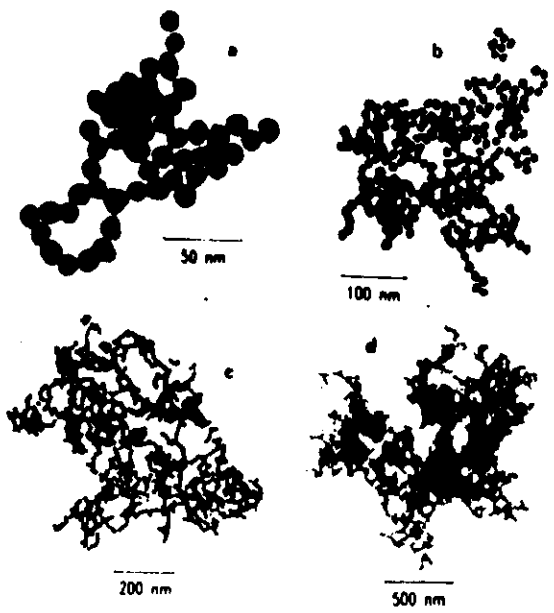

FIGURE 3.6 Transmission electron micrographs of gold clusters of different sizes (Weitz and Huang, 1984)

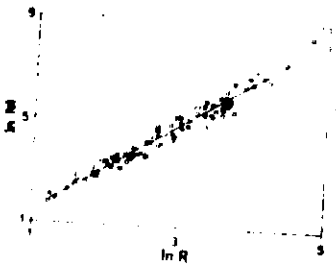

FIGURE 3.7 Variation of the mass as a function of size for gold colloid aggregates. The mass is in units of a single particle mass and the size is scaled by units of the particle diameter. The line corresponds to a fractal dimension $D = 1.7 \pm 0.1$ (Weitz and Huang, 1984)

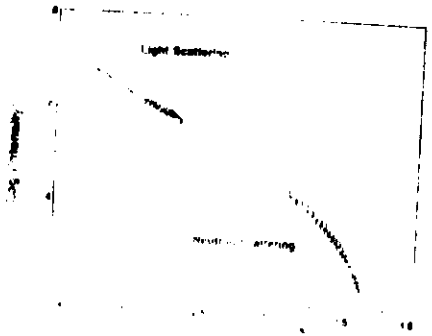

EXPERIMENTAL MEASUREMENTS OF FRACTAL DIMENSION

① DIRECT SPACE

USE OF DEFINITION ON DIGITALIZED MICROGRAPHS

THERE EXIST NOW SOPHISTICATED MICROSCOPE WHICH PROVIDE A SIGNAL ROUGHLY PROPORTIONAL TO THE TRAVERSED MASS.

TWO METHODS

① GREAT NUMBER OF AGGREGATES OF VARIOUS SIZE

TOTAL INTENSITY FUNCTION OF CHARACTERISTIC SIZE

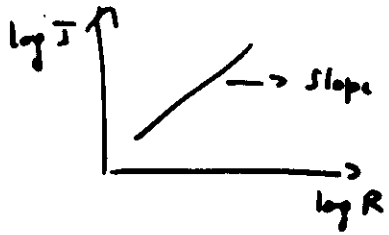

② If one has sufficiently large AGGREGATES

ONE FIRST CHOOSE A GIVEN PARTICLE LOCATED WELL INSIDE THE CLUSTER AND ONE CONSIDERS LARGER AND LARGER PORTIONS (CIRCLE OR SPHERES) OF THE PHOTOGRAPH, CENTERED ON THIS PARTICLE

⚠ PROJECTIONS PROBLEMS.

GENERALLY GOOD IF $D < 2$.

RECIPROCAL SPACE

SCATTERING EXPERIMENT (NON DESTRUCTIVE)

X-ray, Neutron, light.

$$I(q) = I_0(q)\left[1 + \int_0^{\infty} P(r)\,\frac{\sin qr}{qr}\,dr\right]$$

$$|q| = \frac{4\pi}{\lambda}\sin\frac{\theta}{2}$$

$I_0(q)$ Simple particle

$P(r)$ distance distribution function

$P(r)dr$ proport. to the number of interparticle distances between $\vec{r}$ et $\vec{r}+d\vec{r}$

proport to $r^{d-1}\rho(r)$

$\rho(r)$ interparticle correlation function.

$I(0) = N I_0(0)$ Normalization.

THREE DIFFERENT REGIMES (L Size of aggregate)

① $\lambda \gg L$ $(q \ll L^{-1})$

Beam Scattered by the whole aggregate

$$I(q) \simeq I_0(q)\left(1 - \frac{q^2 R_g^2}{3} + \dots\right)$$

② $a \ll \lambda \ll L$

$I(q)$ in $A q^{-D}$

log. log plot.

③ q in a^{-1} Porod regime.

Scattering by individual particles

$I(q) \simeq B q^{-4}$.

ANOMALOUS BEHAVIOUR OF THE A.C. CONDUCTIVITY NEAR PERCOLATION THRESHOLD CAN BE SUMMARIZED IN THE FOLLOWING WAY.

- FOR d.c. CONDUCTIVITY

p	σ
$1-p$	$\sigma = 0$

$$\bar{\sigma} = \sigma (p - p_c)^t$$

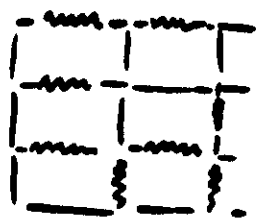

PERCOLATION TRANSITION IS A SECOND ORDER PHASE TRANSITION

$$\frac{T - T_c}{T_c} \quad \text{---} \quad \frac{p - p_c}{p_c}$$

MIXTURE

p	σ_1
$1-p$	$\sigma_2 \ll \sigma_1$

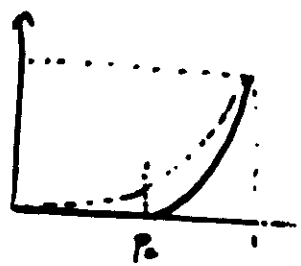

SCALING BEHAVIOUR

$$\bar{\sigma} = \sigma_1 |p - p_c|^t F_\pm \left[\left(\frac{\sigma_2}{\sigma_1} \right)^h |p - p_c|^{-(s+t)} \right]$$

The scaling function $F_\pm$ $+ > p_c$ $- < p_c$ has different asymptotic values

$$\bar{\sigma} = \sigma_1 |p - p_c|^t F_\pm \left[\frac{\sigma_2}{\sigma_1} (p - p_c)^{-t-s} \right]$$

if $\sigma_2 \to 0$, $p > p_c$ $\quad F_+ [x \to 0] \to 1$

$$\bar{\sigma} = \sigma_1 |p - p_c|^t$$

if $\sigma_1 \to \infty$ (supercond.)

$$F_- [x \to 0] \to x$$

$$\sigma_1 |p - p_c|^t \frac{\sigma_2}{\sigma_1} |p - p_c|^{-t-s}$$

$$\sigma_2 |p - p_c|^{-s} \qquad s \text{ supercond. exponent}$$

$$\xi = \xi_1 |p - p_c|^{-s}$$

if $p - p_c \to 0$ $\quad F_\pm (x \underset{x \to \infty}{\to}) = x^u \qquad u$?

$$\bar{\sigma} = \sigma_1 |p - p_c|^t \left[\frac{\sigma_2}{\sigma_1} (p - p_c)^{-t-s} \right]^u$$

$$\bar{\sigma} = \sigma_1 |p - p_c|^{t - (t+s)u} \left(\frac{\sigma_2}{\sigma_1} \right)^u$$

$$\| \; 0$$

$$u = \frac{t}{t+s}$$

one has also $x \to \infty$ if $\sigma_2 \gg (p - p_c)^{t+s} \sigma_1$

close to $p = p_c$

$$\bar{\sigma} \sim \sigma_1 \left(\frac{\sigma_1}{\sigma_2} \right)^{\frac{t}{s+t}}$$

$$\xi \sim \xi_1 \left(\frac{\xi_1}{\xi_2} \right)^{\frac{s}{s+t}}$$

42

If $\sigma_2 \to 0 \quad p \to p_c^+$

$$\sigma = \sigma_1 (p - p_c)^t$$

if $\sigma_1 \to \infty \quad p \to p_c^-$

$$\sigma = \sigma_2 (p - p_c)^{-s}$$

upon analytical continuation $\varepsilon_2 \to \varepsilon' + \frac{i\sigma}{\varepsilon_0 \omega}$

$$\varepsilon = \varepsilon_2 (p - p_c)^{-s} \qquad p \geq p_c$$

If $p \to p_c$ $\quad \sigma_1 (p - p_c)^{t+s} \ll \sigma_2 \ll \sigma_1$

$$\bar{\sigma} \sim \sigma_1 \left(\frac{\sigma_2}{\sigma_1} \right)^{\frac{t}{s+t}}$$

$\sigma_1 \to \infty$ AND CAPACITANCE $\varepsilon_2 (\sigma_2 = i\omega \varepsilon_0 \varepsilon_2)$

$$\bar{\sigma} = \sigma_1 |p - p_c|^t F_\pm \left[\frac{i\omega}{\omega_0} |p - p_c|^{-(t+s)} \right]$$

$$\omega_0 = \frac{\sigma}{\varepsilon \varepsilon_0}$$

$$\omega \ll \omega^* \sim \omega_0 |p - p_c|^{t+s}$$

STATIC

$\omega^* \ll \omega \ll \omega_0$

$$\sigma^* \sim \sigma \left(\frac{\omega}{\omega_0} \right)^{\frac{t}{s+t}}$$

$$\varepsilon^* \sim \varepsilon \left(\frac{\omega}{\omega_0} \right)^{-\frac{s}{s+t}}$$

J. Phys. C: Solid State Phys. 21 (1988) 1839–1847. Printed in the UK

Percolation and anomalous conduction on fractals in fluid-saturated porous media

F Brouers†‡ and A Ramsamugh†

† Department of Physics, University of the West Indies, Mona, Jamaica
‡ International Centre for Theoretical Physics, Trieste, Italy

Received 31 March 1987, in final form 7 September 1987

Abstract. At low frequency the conductivity of fluid-saturated porous media varies with porosity as φ^m where m is Archie's exponent. At higher frequencies, the real part of the conductivity exhibits a dispersive (non-Gaussian) behaviour characterised by the power law $\sigma'(\omega) \propto \omega^x$. The real part of the dielectric constant, which can attain a very large value at low frequency, varies in the dispersive region as $\varepsilon'(\omega) \propto \omega^{-y}$ with $x + y = 1$. We obtained the values of these exponents from data on brine-saturated porous alumina ceramics presented in previous papers and we determine the values of t and s, the usual conductivity and superconductivity exponents. They agree with the latest theoretical estimations.

The conclusion of our analysis is that the low-frequency conductivity of porous alumina ceramics saturated with saline water yields a value for Archie's exponent compatible with the theory of percolation, while the dielectric constant and the conductivity frequency exponents in the dispersive region are consistent both with percolation theory and with an interpretation in terms of anomalous conduction on fractals.

1. Dielectric enhancement and critical behaviour of the conductivity in composite materials

In brine-saturated porous media a low-frequency dielectric enhancement has been observed. The dielectric constant ε' can attain gigantic values, of the order of 10^4. The effect has been explained in terms of geometrical effects (Sen 1981a, b; Brouers *et al* 1987) as well as electrochemical effects (Chew and Sen 1982). In the discussion of this phenomenon, an analogy with the well known dielectric enhancement occurring in inhomogeneous mixtures of metals and insulators has been put forward. This effect appears when the conducting metallic phase is close to the percolation threshold.

Decisive progress has been made for such systems in developing scaling theories to predict the behaviour of the conductivity σ and the dielectric constant ε' as a function of the volume fraction φ of the conducting material and the frequency ω (Efros and Shklovskii 1976, Bergman and Imry 1977, Webman *et al* 1977, Stroud and Bergman 1982, Wilkinson *et al* 1983, Luck 1985, Laugier *et al* 1986, Clerc *et al* 1985, Granan *et al* 1981). Results of interest here predict that the low-frequency conductivity vanishes at the percolation threshold φ_0 according to a power law of the form

$$\sigma \sim \sigma_\infty (\varphi - \varphi_0)^t \qquad \varphi > \varphi_c$$
$$\sigma = 0 \qquad \varphi < \varphi_c \qquad (1)$$

0022-3719/88/091839 + 09 $02.50

where σ_w is the conductivity of the conducting phase, which is the water in the case of brine-saturated porous media.

At the percolation threshold, the percolation correlation length ξ diverges as

$$\xi \sim |\varphi - \varphi_c|^{-\nu} \qquad \text{for } \varphi > \varphi_c \text{ and } \varphi < \varphi_c. \tag{2}$$

The real part of the dielectric constant is predicted to diverge as φ approaches φ_c:

$$\varepsilon' \sim \varepsilon'_m |\varphi - \varphi_c|^{-s} \tag{3}$$

where ε'_m is the dielectric constant of the matrix. The above results (1) and (2) hold for low frequencies

$$\omega \ll |\varphi - \varphi_c|^{s+t} \sigma_w / \varepsilon'_m \varepsilon_0 \tag{4}$$

where ε_0 is the permittivity of the vacuum. In other words, for $\omega \ll \omega_\xi \sim \xi^{-(s+t)/\nu}$ where $\xi \sim |\varphi - \varphi_c|^{-\nu}$ is the percolation correlation length and ω_ξ^{-1} the diffusion time for a particle to diffuse over a distance ξ, one has $\sigma(0) \sim \xi^{-t/\nu}$ for concentrations of conducting material above the percolation threshold $\varphi > \varphi_c$ and $\varepsilon'(0) \sim \xi^{s/\nu}$ for $\varphi < \varphi_c$ and $\varphi > \varphi_c$. It should be noted that the dielectric constant discussed in this work, as well as in quoted work, is that at zero wavenumber k, i.e. the quantity $\varepsilon(\omega) = \lim_{k \to 0} \varepsilon(k, \omega)$. The above exponents describe macroscopic averages taken over samples that are larger than the correlation length ξ.

By contrast for

$$\omega \gg |\varphi - \varphi_c|^{s+t} (\sigma_w / \varepsilon'_m \varepsilon_0) \tag{5}$$

that is

$$\omega \gg \omega_\xi \sim \xi^{-(s+t)/\nu} \sim |\varphi - \varphi_c|^{s+t} \tag{6}$$

the dielectric constant ε' increases as the frequency is lowered following the law

$$\varepsilon' \sim \varepsilon'_m |\sigma_w / \varepsilon'_m \varepsilon_0 \omega|^{(s+t)/(s+t)} \sim \omega^{-(s+t)/(s+t)} \tag{7a}$$

while the AC conductivity varies as

$$\sigma \sim \omega^{t/(s+t)}. \tag{7b}$$

In (1), (3) and (7) the exponents t and s are the usual conductivity and superconductivity exponents. These exponents are universal, i.e. they do not depend on details of the geometry such as grain shape or coordination number, but only on the space dimension of the system. Values generally quoted are $s = t \simeq 1.3$ in two dimensions and $s \simeq 0.7$ and $t \simeq 1.8$ in three dimensions. More recent evaluations (Balberg *et al* 1983, Balberg and Bozowski 1982, Derrida *et al* 1983) yield $t_2 \simeq 1.25$ and $t_3 \simeq 1.95$ and $s_3 \simeq 0.75$ (Herrmann *et al* 1984).

The scaling laws (7) are related to the self-similar properties of these systems. Self-similarity is an essential aspect of percolation at threshold. The self-similarity region broadens at finite frequencies. For $\omega \gg \omega_\xi$, near φ_c in the corresponding length range $a \ll L \ll \xi$, where a is a microscopic length limit, the system has a self-similarity (fractal) geometry, i.e. many physical quantities scale as a power law of the length scale L on which they are measured. In the corresponding frequency range $\omega_\xi < \omega < \omega_a$ where ω_a is a frequency determined by a microscopic distance a, below which the response is determined by the microscopic behaviour of the system, anomalous conduction referred to as 'anomalous conduction on fractals' occurs and the (real part of the) conductivity

and the (real part of the) dielectric constant follows the power law

$$\sigma'(\omega) \sim \omega^x \qquad x = t/(s+t) \tag{8a}$$

$$\varepsilon'(\omega) \sim \omega^{-y} \qquad y = s/(s+t) \tag{8b}$$

and

$$x + y = 1. \tag{8c}$$

The behaviour (8*a*) corresponds to a dispersive (non-Gaussian) transport for which the time-dependent mean square distance

$$\langle \Delta r^2(\tau) \rangle = \langle (r(\tau) - r(0))^2 \rangle$$

increases sublinearly with time τ.

For $\omega < \omega_\xi$ the conduction is classical and yields a constant conductivity σ. For $\omega > \omega_a$, the conductivity is determined by the microscopic response of the conductive grains (Laibowitz and Gefen (1984)).

It must be noted that the anomalous diffusion in independent percolation clusters when capacitance on bonds connecting different clusters is neglected is different from that described by (8) (Gefen *et al* 1983).

2. Critical behaviour in fluid-saturated porous media

The motivation for this work is the phenomenon of dielectric enhancement in porous rocks containing salty (i.e. conducting) water. Although a low-frequency dielectric enhancement is indeed observed in porous rocks (Sen 1981a, b), the results we have discussed in § 1 strictly refer only to random systems. Such systems always exhibit a non-zero percolation threshold φ_c below which the DC conductivity vanishes.

In reality, in brine-saturated porous rocks where the phenomenon of low-frequency dielectric enhancement is observed, the empirical law known as Archie's Law (Archie 1942, Sen *et al* 1981)

$$\sigma \sim \sigma_w \varphi^m \tag{9}$$

indicates that $\varphi_c = 0$, i.e. the water in the pore space remains conducting down to arbitrarily low porosities. If we assume that the pore space is completely filled with water, this means geometrically that the pore space remains connected even in samples with very low porosity.

One of the key properties of the dielectric enhancement for random systems is the universal behaviour in the critical region. Presumably, the analogue for rocks of the limit $\varphi \to \varphi_c$ is the low-porosity limit.

The question is raised of whether or not Archie's law can be explained by ordinary percolation in the continuum (i.e. is this theory consistent with the very small critical porosity φ_c and with the observed values of m?) Although a corresponding universality would explain the wide applicability of Archie's law with $m \simeq 2$, it remains to be proved that such universality exists with respect to variations such as grain shape and packing geometry. If percolation theory could be applied to interpret Archie's law this would have the advantage of being based on universal behaviour and of not requiring *a priori* assumptions regarding the microstructure of the pores in the materials, as other theories do. This would be extremely useful for geophysical and materials science studies if there

exist universal laws governing dielectric and conductivity properties of fluid-saturated porous media. Indeed in the iterated effective-medium approximation proposed by Sen *et al* (1981) and Mendelson and Cohen (1982), the exponent m depends on grain shape. However the exponents are controlled by the dilute-rock limit and there is no guarantee that the results are still valid in the low-porosity regime where the rock grains are touching.

In a recent paper Balberg (1986) using a model of soft-core pores in an insulating matrix has shown that in rocks where the pores have a large aspect ratio the onset of percolation can occur for a very small pore space. (Similar conclusions can be obtained by calculating the percolation threshold in mean-field theories; see Brouers (1986).) Arguing that the consideration of the neck size distribution and the degree of anisotropy can allow one to account for the distribution of m observed, Balberg (1986) concluded that ordinary percolation theory provides a realistic model for the pore space in rocks and is more general than effective-medium and fractal theories.

Unfortunately, to the best of our knowledge there are no published data correlating the exponents m, s and t systematically on porous materials. The present paper is one of the first reporting frequency-dependent dielectric and electrical conductivity data allowing such an analysis.

3. Critical exponents in brine-saturated porous alumina ceramics

In a series of papers (Brouers and Ramsamugh 1986, Brouers *et al* 1987, Ramsamugh and Brouers 1987) we have discussed measurements of the electrical conductivity and the dielectric constant of brine-saturated porous alumina ceramics. The aim of that work was to investigate the relation between the pore geometry and the frequency variation of these two quantities with salinity and porosity, discussed mostly in geophysical journals dealing with the physics of rocks and soils.

In the first of our series of papers (Brouers and Ramsamugh 1986), we discussed the relation between conductivity and fluid flow permeability in porous alumina ceramics.

In a second paper (Brouers *et al* 1987) we discussed the phenomenon of dielectric enhancement in brine-saturated ceramics. Large values of the real part of the dielectric constant ε' of the order of 10^6 are observed at low frequencies while the samples remain conducting. At low and high frequencies the conductivity is independent of frequency. In a frequency range that depends on salinity and porosity, the fluid-saturated porous alumina ceramics exhibit a frequency dependence

$$\sigma'(\omega) \propto \omega^n \tag{10}$$

where $n < 1$. This is compatible with the 'universal' pattern of behaviour discussed by Jonscher (1977). In that paper (Brouers *et al* 1987) we were able to show that a model of ramified clusters of elongated dead-end pores encased in shells of insulating rocks could provide a possible or partial explanation of the electrolyte-saturated ceramic dielectric and conductivity data.

In a subsequent paper (Ramsamugh and Brouers 1987), an empirical scaling law for the real part of the frequency-dependent electrical conductivity $\sigma'(\omega)$ of brine-saturated porous materials in relation to its DC limit was identified. The scaling law relates the conductivity as a function of frequency, porosity and salinity to a function of only one variable that is the ratio of the frequency to the DC conductivity in appropriate units; it

Table 1. The dielectric constant and conductivity exponents of equations (8a) for various porosities and salinities. The values of s were obtained by identifying m with t and from the ratios of the values in columns 4 and 5.

Salinity (wt %)	Porosity	m	$s/(s+t)$	$t/(s+t)$	s
	0.179		0.28	0.79	0.60
	0.193		0.24	0.79	0.59
0.4	0.253	1.94	0.29	0.72	0.78
	0.275		0.27	0.74	0.71
	0.433		0.27	0.72	0.73
	0.179		0.29	0.79	0.70
	0.193		0.30	0.74	0.78
2.0	0.253	1.92	0.30	0.70	0.82
	0.275		0.26	0.79	0.63
	0.433		0.29	0.77	0.72
	0.179		0.30	0.74	0.79
	0.193		0.30	0.77	0.76
4.0	0.253	1.95	0.29	0.71	0.80
	0.275		0.24	0.75	0.62
	0.433		0.29	0.74	0.76
	0.179		0.30	0.75	0.77
	0.193		0.30	0.76	0.76
5.6	0.253	1.92	0.28	0.70	0.77
	0.275		0.27	0.72	0.72
	0.433		0.31	0.72	0.83

can be written as

$$\sigma'(\omega)/\sigma(0) = f(A\varepsilon_0\omega/\sigma(0)) \tag{11a}$$

where

$$f(x) = 1 + x^{0.745} \tag{11b}$$

over the main part of the non-Gaussian frequency range and A is a constant which depends on salinity porosity and possibly on temperature. This result is very similar to what has been reported in hopping semiconducting systems.

The results of Brouers *et al* (1987) allow a complete discussion of the exponents m, $t/(s+t)$ and $s/(s+t)$ for the set of porous alumina ceramics considered in this paper. We have measured the slope of $\sigma'(\omega)$ and $\varepsilon'(\omega)$ in the self-similarity frequency range. These values are reported in table 1 for porosities 0.179, 0.193, 0.253, 0275, 0.433. In figures 1 and 2, we present the experimental data for the dielectric constant and electrical conductivity for an intermediate porosity $\varphi = 0.193$ not included in the curves shown by Brouers *et al* (1987).

The value of the Archie's law, dielectric constant and conductivity exponents m, $s/(s+t)$ and $t/(s+t)$ are respectively 1.94, 0.284 and 0.746. (In one of our earlier papers (Brouers and Ramsamugh 1986), the measurements of m were made at 10^3 Hz. Here they correspond to 10 Hz.) The sum of the last two exponents is 1.03 and the standard deviation of the data of table 1 is 0.03. This is in agreement with (8c). The value of m is very close to the percolation theory values of Balberg *et al* (1983), Balberg and Bozowski (1982) and Derrida *et al* (1983).

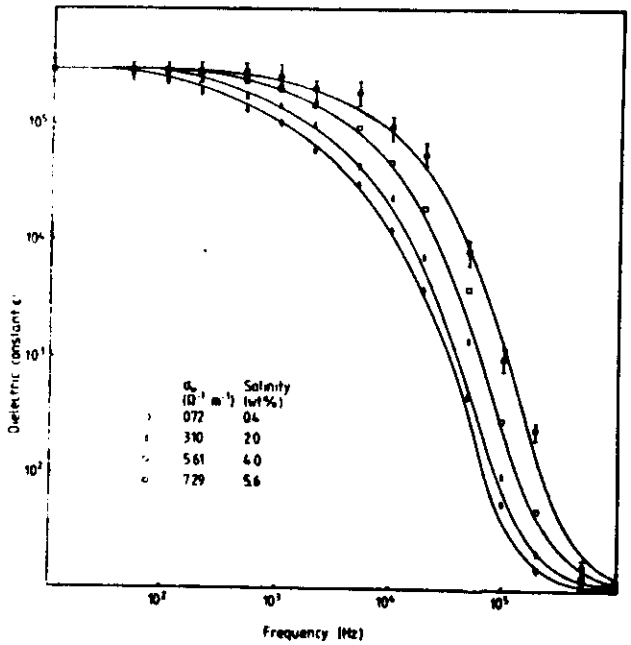

Figure 1. The frequency dependence of the real part of the dielectric constant of brine-saturated alumina ceramics of porosity = 0.193 for four different salinities. ε' for dry alumina is 8.90.

If the Archie's law exponent m is identified with the percolation theory conductivity exponent t, our data yield a value of $s = 0.73 \pm 0.06$ in agreement with theoretical results ($s_3 = 0.75 \pm 0.04$) of Herrmann *et al* (1984) and the experimental measurement ($s_3 = 0.73 \pm 0.07$) of Bowman and Stroud (1984).

4. The fractal dimension

A fractal dimension d_f can be determined using theoretical expressions derived for percolating clusters. If we use the relations between the exponents t, s, ν, d_f and the random walk dimension d_{rw} established by Alexander and Orbach (1982) and Coniglio and Stanley (1984) (see also Niklasson and Granqvist 1986) i.e.

$$t/\nu = 1 + d_{rw} - d_f \tag{12a}$$

and

$$s/\nu = (d_f - 1)/2 \tag{12b}$$

we can calculate d_f and d_{rw} noting, however, that (12*a*) is exact and (12*b*) still a conjecture. The exponent ν can be determined first, using the 'hyperscaling law' proposed by

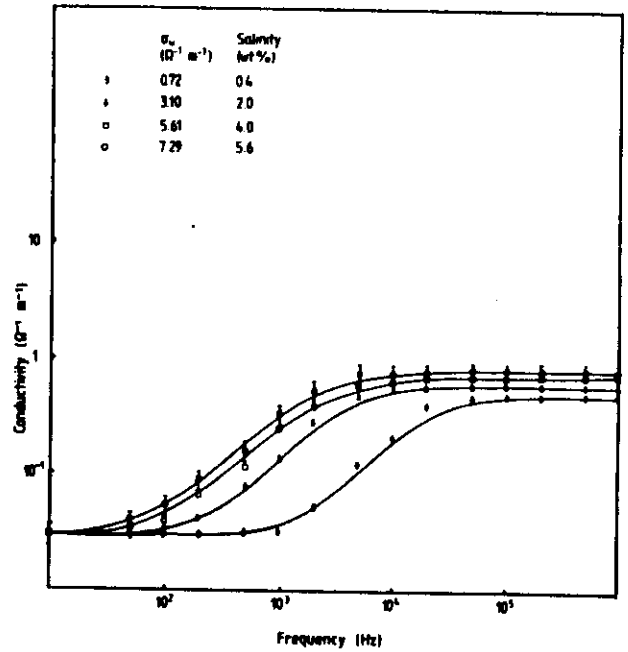

Figure 2. The frequency dependence of the electrical conductivity of brine-saturated alumina ceramics of porosity = 0.193 for four different salinities.

Straley (1980):

$$t + s = d\nu. \tag{13}$$

The average value $\nu = 0.89 \pm 0.02$ is in agreement with the value of 0.88 ± 0.02 given by Gaunt and Sykes (1983) and the value of 0.87 ± 0.02 given by Hermann *et al* (1984).

The values of d_f and d_{rw} are given in table 2. In the last column we give the values of the spectral dimension

$$d_s = 2d_f/d_{rw} \tag{14}$$

which are slightly higher than the Alexander and Orbach (1982) conjecture of $\frac{4}{3}$.

5. Discussion

We have found that the critical exponents s, t, ν and the relations between the dimensions d_f, d_{rw}, d_s of brine-saturated porous alumina ceramics are consistent with percolating models. This may strengthen the recent proposal by Balberg (1986) that 'ordinary percolation provides a realistic model for the pore space'. However, it must be kept in mind, as discussed in § 2, that the porosities (up to 40%) are far from the percolation threshold ($\varphi_c = 0$). The fact that $\varphi_c = 0$ presumably means that the pore network

Table 2. The conductivity t and superconductivity s exponents from table 1. The correlation length exponents ν were obtained from equation (13). The fractal, random walk and spectral dimensions d_f, d_w and d_s were obtained from equations (12) and (14).

Porosity, q	t	s	ν	d_f	d_w	d_s
0.179	1.94	0.72	0.89	2.64	3.79	1.39
0.193	1.94	0.72	0.89	2.64	3.79	1.39
0.253	1.94	0.79	0.91	2.74	3.87	1.41
0.275	1.94	0.67	0.87	2.54	3.77	1.35
0.433	1.94	0.76	0.90	2.69	3.84	1.42
Average value	1.94	0.73	0.89	2.65	3.81	1.39

geometry is dominated by the formation mechanism and is not at all random. It is now known that fractal growth models can explain the fractal nature of ceramics and that diffusion-limited aggregation and other related models (Schaefer and Keefer 1986) may have a fractal dimension and other exponents rather close to those of percolation clusters.

On the other hand, if one follows the controversial suggestion (Katz and Thompson 1985) that the pore volume behaves as a fractal with the fractal dimension of the pore–grain interface, the value $d_f = 2.65 \pm 0.10$ obtained. This is very close to the value of the alumina surface fractal dimension $d_f = 2.79 \pm 0.03$ obtained by Avnir *et al* (1984) and Pfeifer (1986) from an analysis of molecular adsorption on porous alumina ceramics. The determination of the fractal dimension of a rough surface by Monte Carlo simulations by Mon (1986) for a solid-on-solid model above the roughening transition, also gives a similar value, namely $d_f = 2.8 \pm 0.03$.

Low-frequency conductivity and dielectric measurements can provide useful information on the fractal and anomalous transport in porous media. However, before one can make definite statements on the validity of the various competing models, a more detailed morphological analysis must be performed.

Acknowledgments

We would like to thank Dr Duvigneaud of the Laboratoire de Chimie Industrielle, Université Libre de Bruxelles, who has prepared the samples. We are grateful to the referees for useful comments and suggestions. One of us (FB) would like to thank Professor Abdus Salam, the International Atomic Energy Agency and Unesco for their hospitality at the International Centre for Theoretical Physics, Trieste. This work was supported by a grant from the Third World Academy of Science.

References

Alexander S and Orbach R 1982 *J. Phys. Lett.* **43** L625
Archie G E 1942 *Trans. AIME* **46** 54
Avnir D, Farin D and Pfeifer P 1984 *Nature* **308** 261
Balberg I 1986 *Phys. Rev.* B **33** 3618
Balberg I, Bienenbaum N and Anderson C H 1983 *Phys. Rev. Lett.* **51** 1605

Balberg
Bergma
Bowma
Brouer
Brouer
Brouer
Chew W
Clerc J
Coniglio
Derrida
Efros A
Gaunt
Gefen
Granan
Herrma
Jonsche
Katz A
Laibowi
Laugier
Luck J
Mendel
Mon K
Niklass
Pfeifer
Ramsan
Schaefe
D E
Sen P N
—
Sen P N
Stroud
Straley
Wilkins
Webman

Balberg I and Bozowski S 1982 *Solid State Commun.* **44** 551
Bergman D J and Imry Y 1977 *Phys. Rev. Lett.* **39** 1222
Bowman D R and Stroud D 1984 *Phys. Rev. Lett.* **52** 299
Brouers F 1986 *J. Phys. C: Solid State Phys.* **19** 7183
Brouers F and Ramsamugh A 1986 *Solid State Commun.* **60** 951
Brouers F, Ramsamugh A and Dixit V V 1987 *J. Mater. Sci.* **22** 2759
Chew W C and Sen P N 1982 *J. Chem. Phys.* **77** 4683
Clerc J P, Giraud G, Laugier J M and Luck J M 1985 *J. Phys. A: Math. Gen.* **18** 2565
Coniglio A and Stanley H E 1984 *Phys. Rev. Lett.* **52** 1068
Derrida B, Stauffer D, Herrmann H J and Vannimenus J 1983 *J. Physique Lett.* **44** L701
Efros A L and Shklovskii B I 1976 *Phys. Status Solidi* b **76** 475
Gaunt D S and Sykes M F 1983 *J. Phys. A: Math. Gen.* **16** 783
Gefen Y, Aharony A and Alexander S 1983 *Phys. Rev. Lett.* **50** 77–80
Granan D M, Garland J C and Tanner D B 1981 *Phys. Rev. Lett.* **46** 375–8
Herrmann H J, Derrida B and Vannimenus J 1984 *Phys. Rev.* B **30** 4080
Jonscher A K 1977 *Nature* **267** 673
Katz A J and Thompson 1985 *Phys. Rev. Lett.* **54** 1325
Laibowitz R B and Gefen Y 1984 *Phys. Rev. Lett.* **53** 380
Laugier J M, Clerc J P, Giraud G and Luck J M 1986 *J. Phys. A: Math. Gen.* **19** 3153
Luck J M 1985 *J. Phys. A: Math. Gen.* **18** 2061
Mendelson K S and Cohen M H 1982 *Geophysics* **47** 257
Mon K K 1986 *Phys. Rev. Lett.* **57** 866
Niklasson G A and Granqvist C G 1986 *Phys. Rev. Lett.* **56** 256
Pfeifer P 1986 *Fractals in Physics* ed. L Pietronero and E Tosatti (New York: Elsevier) p 47
Ramsamugh A and Brouers F 1987 *Phil. Mag. Lett.* **55** 301
Schaefer D W and Keefer K D 1986 *Better Ceramics Through Chemistry Proc. MRS Symp.* ed. C J Brinker, D E Clarck and D R Ulrich (Amsterdam: North-Holland)
Sen P N 1981a *Appl. Phys. Lett.* **39** 667
—— 1981b *Geophysics* **46** 1714
Sen P N, Scala C and Cohen M H 1981 *Geophysics* **46** 781
Stroud D and Bergman D J 1982 *Phys. Rev.* B **25** 2061
Straley J P 1980 *J. Phys. C: Solid State Phys.* **13** 819
Wilkinson D, Langer J S and Sen P N 1983 *Phys. Rev.* B **28** 1081
Webman I, Jortner J and Cohen M H 1977 *Phys. Rev.* B **16** 2593